Editors' choice

Vertebral, rib, and osteoderm morphology and histology of Middle Triassic diapsid *Eusaurosphargis*

NICOLE KLEIN and TORSTEN M. SCHEYER

Klein, N. and Scheyer, T.M. 2024. Vertebral, rib, and osteoderm morphology and histology of Middle Triassic diapsid *Eusaurosphargis*. *Acta Palaeontologica Polonica* 69 (4): 633–648.

Bone histology and microanatomy of neck and dorsal vertebrae, a dorsal rib, and osteoderms from different body regions of *Eusaurosphargis* aff. *dalsassoi* from Winterswijk, The Netherlands, are studied by petrographic thin sections and micro-computed tomographic (μCT) data. Osteohistology in the axial elements differs from that of marine reptiles and corroborates a terrestrial or semiaquatic life style for *Eusaurosphargis* aff. *dalsassoi*. Not only the outer shape and overall microanatomy of the osteoderms, but also the association and attachment of the osteoderms to the underlying endoskeletal element (i.e., cervical vertebra, rib, appendicular element) vary depending on body region. Furthermore, chondroid bone is identified in the osteoderms of *Eusaurosphargis* aff. *dalsassoi*, which is the oldest evidence of this tissue in osteoderms of an extinct tetrapod. For comparison, μCT data of two neural arches tentatively identifiable as pertaining to the enigmatic Middle Triassic *Saurosphargis voltzi* (the holotype and only specimen of this taxon is considered lost) could be included. They share with *Eusaurosphargis* aff. *dalsassoi* the elongated transverse processes and a general similar microstructure, but also present an anteroposteriorly broadened bony sheath of the transverse process in ventral view, which is absent in *Eusaurosphargis* aff. *dalsassoi.*

Key words: Eureptilia, Triassic, Winterswijk, Muschelkalk, osteoderms, palaeohistology, chondroid bone.

Nicole Klein [nklein@posteo.de; ORCID: https://orcid.org/0000-0003-3638-1194], Institut für Geowissenschaften, Paläontologie, Universität Bonn, Nußallee 8, 53115 Bonn, Germany.
Torsten M. Scheyer [tscheyer@pim.uzh.ch; ORCID: https://orcid.org/0000-0002-6301-8983], University of Zurich, Department of Paleontology, Karl Schmid-Strasse 4, CH-8006 Zurich, Switzerland.

Received 18 April 2024, accepted 13 September 2024, published online 19 December 2024.

Introduction

The monospecific, small to medium sized (<1 m as adult) *Eusaurosphargis dalsassoi* Nosotti & Rieppel, 2003, is exclusively known from the Middle Triassic (Anisian–Ladinian) of the western Tethyan realm, i.e., the Alpine Triassic (Nosotti and Rieppel 2003; Scheyer et al. 2017) and the Germanic Basin (Klein and Sichelschmidt 2014; Scheyer et al. 2019). This taxon is generally considered to be a rare faunal component, but due to its characteristically elongated transverse processes (abbreviated as tp thereafter) of the dorsal vertebrae, ribs having uncinate processes associated with an osteoderm, and additional osteoderms covering much of the vertebral spine and appendicular skeleton, it is relatively easy to identify. From the Alpine region, *E. dalsassoi* is known by the holotype, a disarticulated subadult specimen from the Besano Formation (Middle Triassic, Anisian–Ladinian), Italy (Nosotti and Rieppel 2003), and a slightly smaller, almost fully articulated juvenile specimen from the Prosanto Formation (Middle Triassic, Ladinian), Ducanfurgga, Switzerland (Scheyer et al. 2017). A poorly preserved skeleton from the lower Buchenstein Formation (late Anisian) of Piz da Peres, Dolomites, Northern Italy (Wachtler 2018), was later also identified as another potential juvenile specimen of *E. dalsassoi* (Renesto et al. 2020). From the Germanic Basin, finds that so far could be assigned to *Eusaurosphargis* aff. *dalsassoi* are known from the Vossenveld Formation (Middle Triassic, Anisian) of Winterswijk, The Netherlands (Sander et al. 2014; Scheyer et al. 2019) and from a few other localities from the central and eastern parts of the Germanic Basin (NK, personal observation). The material includes vertebrae, osteoderms, and ribs, as well as isolated cranial material (e.g., Klein and Sichelschmidt 2014; Sander et al. 2014; Willemse et al. 2019).

Despite a recently increasing number of specimens, the phylogenetic position of *E. dalsassoi* is contested: a previous analysis found *Eusaurosphargis* and *Helveticosaurus* as successive sister taxa to Sauropterygia (Scheyer et al. 2017), whereas the latest analysis indicated a sister group

relationship of *Eusaurosphargis* with *Palatodonta bleekeri* as closest sister group to Sauropterygia (Wolniewicz et al. 2023). Neither of these analyses find *Eusaurosphargis* forming a natural group (i.e., a monophyletic clade) with Saurosphargidae, a group of Eusauropterygia known mainly from the Middle Triassic of China, which is also characterized by dorsal vertebrae with elongated transverse processes (Li et al. 2011; Wolniewicz et al. 2023).

Although *Eusaurosphargis* remains are found in shallow marine and/or near coastal sediments, Scheyer et al. (2017) argued for a terrestrial lifestyle based on several morphological features (including limb- and autopodial morphology and long bone microanatomy) and its rareness compared to similar sized unequivocal marine reptiles such as pachypleurosaurs, a view that was later corroborated by a new find (Renesto et al. 2020).

Saurosphargis voltzi Huene, 1936, is a rare faunal component in the Middle Triassic (lower to middle Anisian) of the Germanic Basin (summarized in Scheyer et al. 2019). The holotype and only known specimen, found in sediments indicating a near coastal environment (Gogolin, Poland), consisted of articulated ribs and vertebrae from the trunk region. It was lost during World War II (see Nosotti and Rieppel 2003 on further historical notes on the specimen). The most important morphological characteristic of *S. voltzi* are elongated transverse processes. Before the description of *E. dalsassoi* from the Anisian/Ladinian (Besano Formation) of northern Italy (Nosotti and Rieppel 2003), finds of vertebrae with elongated transverse processes found in the central Germanic Basin (i.e., Muschelkalk sediments) had always been tentatively assigned to *S. voltzi* (summarized in Scheyer et al. 2019). The taxon is considered a nomen dubium by some authors (e.g., Scheyer et al. 2017, 2019) but accepted as valid taxon by others (e.g., Wolniewicz et al. 2023). In any case, on the basis of new taxa described from shallow marine sediments of the Anisian (Middle Triassic) of China (*Sinosaurosphargis yunguiensis* Li et al., 2011, *Largocephalosaurus polycarpon* Cheng et al., 2012, *Largocephalosaurus qianensis* Li et al., 2014), the existence of a clade Saurosphargidae has now been established (Wolniewicz et al. 2023). Based on what is known of *S. voltzi*, there is consensus that the latter and the Chinese taxa share certain characters, making *Saurosphargis* the name-giving taxon of the clade Saurosphargidae Li et al., 2011.

In the current paper, osteohistology and microanatomy of vertebrae, a dorsal rib, and osteoderms of *Eusaurosphargis* aff. *dalsassoi* from the locality of Winterswijk are described to evaluate histological and microanatomical characters that might further elucidate its life style.

Additionally, we were able to study the morphology and microanatomy by μCT data of two articulated neural arches including parts of the osteoderms of dorsal vertebrae of *Saurosphargis* aff. *voltzi*. For a better comparison, μCT data of additional vertebrae of *Eusaurosphargis* aff. *dalsassoi* are included as well. The aim was here to find morphological indications to distinguish both taxa based on their vertebrae. Further on, we wanted to clarify if the elongated transverse processes of *Eusaurosphargis* aff. *dalsassoi* and *Saurosphargis* aff. *voltzi* are only superficially/morphologically convergent or if also the inner structure follows the same or a different developmental pathway.

Institutional abbreviations.—IGPB, Institute of Geosciences, Paleontology, University of Bonn, Germany; NHMS, Natural History Museum Schleusingen, Germany; NMNHL, National Museum of Natural History (NCB Naturalis), Leiden, The Netherlands.

Other abbreviations.—cb, chondroid bone; isf, interwoven structural fiber tissue; pfcb, postcranial fibro-cartilaginous bone; tp, transverse process; wfb, woven bone tissue.

Material and methods

Material of *Eusaurosphargis* aff. *dalsassoi*.—The locality of Winterswijk, The Netherlands exposes the Lower Muschelkalk (Vossenveld Formation; Hagdorn and Simon 2010), which is dated as early Anisian (Middle Triassic). The quarry is located at the formerly eastern part of the Germanic Basin. Sediments are coastal to shallow marine (Dülfer and Klein 2006) and have yielded a diverse vertebrate fauna with some layers preserving many skeletal remains and others preserving some outstanding trackways and footprints. Taxa such as nothosaurs and pachypleurosaurs are represented by high individual numbers (Heijne et al. 2019), whereas other faunal components such as Placodontia, Tanystropheidae, and also *Eusaurosphargis* aff. *dalsassoi* are rare in comparison (summarized in Voeten et al. 2019; Heijne et al. 2019; and Oosterink et al. 2021).

From this locality, two dorsal vertebrae, one from the anterior or posterior trunk region (IGPB Wijk08-153) and one from the mid-trunk region (IGPB Wijk11-394), a dorsal rib (IGPB Wijk10-246), and three osteoderms (IGPB Wijk07-74, IGPB Wijk09-551, IGPB Wijk10-364) of *Eusaurosphargis* aff. *dalsassoi* were thin sectioned (Fig. 1). Both sampled vertebrae were incompletely preserved. From vertebra IGPB Wijk08-153 only the posterior half was available, and the thin sections represent the posterior most part of the tp. IGPB Wijk11-394 was cut along the left preserved tp. The vertebra was largely embedded in sediment when sampled and cut not exactly transversely but somewhat obliquely as is evident from the different angles in which the complete and incomplete tp are visible. The dorsal rib was cut at four places (at proximal shaft, midshaft: anterior to the uncinate process, midshaft at the uncinate process and twice at the distal shaft) transversally to its long/shaft axis (Fig. 1E). One "rib" osteoderm (IGPB Wijk09-551) was thin-sectioned along two parallel planes, one section crossing transversally through the base and the other crossing more dorsally closer to the apex (Fig. 1D). Another "rib" osteoderm (IGPB Wijk10-364)

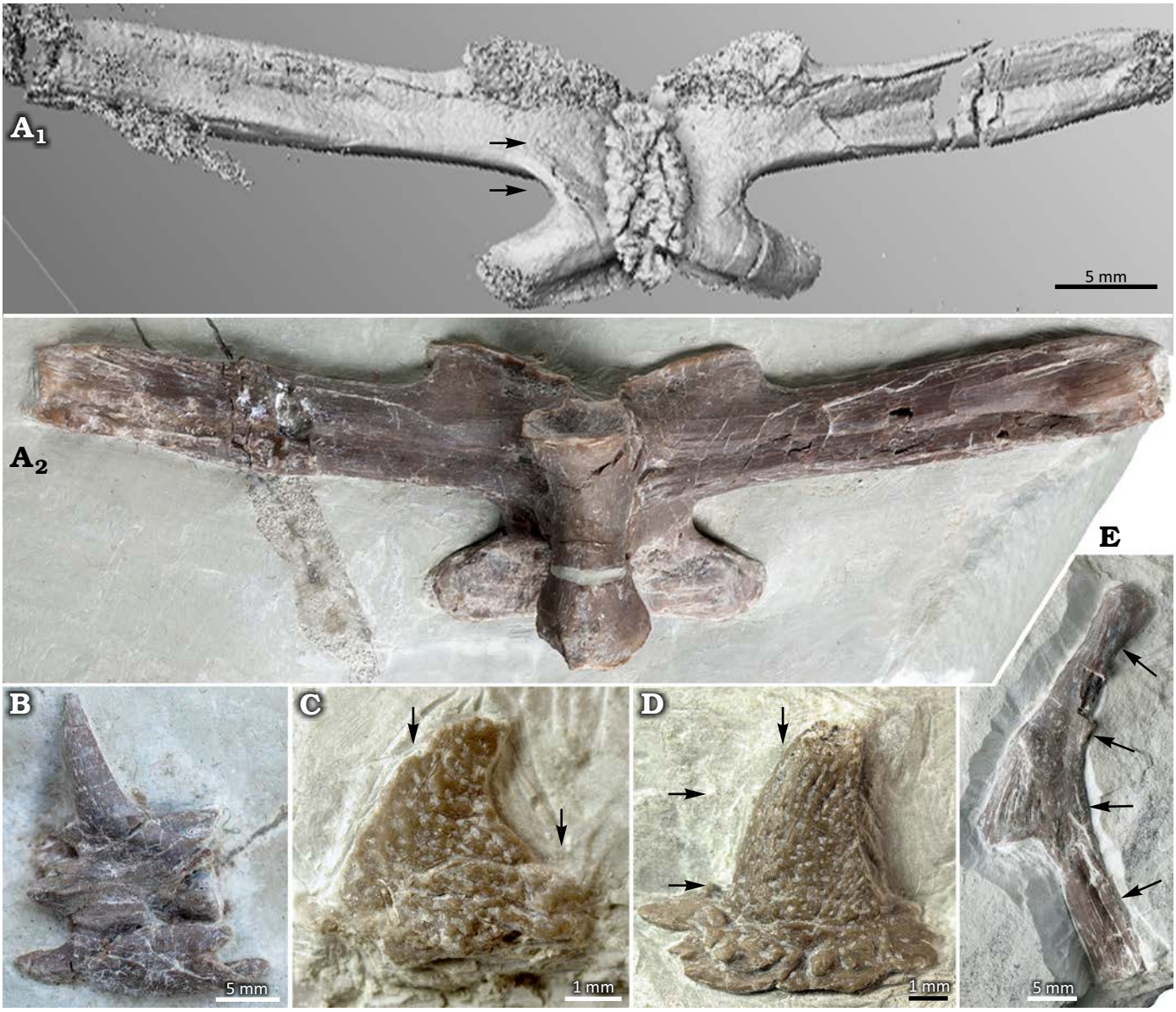

Fig. 1. Sampled elements of *Eusaurosphargis* aff. *dalsassoi* Nosotti & Rieppel, 2003, from Winterswijk, The Netherlands; Lower Muschelkalk, Vossenveld Formation, lower Anisian (Middle Triassic). Please note that the thin sectioned vertebrae IGPB Wijk08-153 and IGPB Wijk11-394 are not figured. **A**. IGPB Wijk06-110. A_1, µCT image of dorsal vertebra (mid-trunk region) in dorsal view; note the very flat osteoderm (as a rugosity) that covers the neural spine; A_2, photograph in ventral view. **B**. Neck vertebra IGPB Wijk10-231 with a spiky osteoderm sitting on the neural arch and left cervical rib attached to the centrum. **C**. "Appendicular" osteoderm IGPB Wijk07-74. **D**. "Rib" osteoderm IGPB Wijk09-551. **E**. Dorsal rib IGPB Wijk10-246; arrows mark the respective planes of thin sections.

was cut parasagittally. The "appendicular" osteoderm (IGPB Wijk07-74) was sectioned parasagittally, too (Fig. 1C).

The rib (IGPB Wijk10-246), one neck vertebra including its osteoderm (IGPB Wijk10-231), a dorsal vertebra with osteoderm (IGPB Wijk06-110), and the "rib" osteoderm (IGPB Wijk09-551) had been scanned using micro-computed tomography (µCT).

Material of *Saurosphargis* aff. *voltzi*.—Two articulated but heavily compressed neural arches of dorsal vertebrae (NHMS WT 647) from the Lower Muschelkalk (Anisian) of the Themar quarry near Schleusingen (Thuringia, Germany) were available for micro-computed tomography.

Methods.—Petrographic thin sections were prepared according to the method described in Klein and Sander (2007). The histological study was performed with a Leica DM LP microscope, the images were obtained with a Leica DFC 420 and an EOS Canon camera. Some images were taken with a Keyence vhx-7000 digital microscope. The histological nomenclature follows Francillon-Vieillot et al. (1990) and Buffrénil et al. (2021).

µCT scans were recorded with a v|tome|x s scanner manufactured by GE phoenix|X-ray (Wunstorf, Germany). The µCT machine is operated by the IGPB.

The image stack of the neck vertebra (IGPB Wijk10-231)

consists of 1000 images and was recorded at a voltage of 140 kV and a current of 110 mA, yielding a voxel size of 31.71 µm. The image stack of the dorsal vertebra (IGPB Wijk06-110) consists of 1500 images and was recorded at a voltage of 120 kV and a current of 110 mA, yielding a voxel size of 55.2 µm. The image stack of the neural arches of *Saurosphargis* aff. *voltzi* (NHMS WT647) consists of 1000 images and was recorded at a voltage of 180 kV and a current of 110 mA, yielding a voxel size of 57.14 µm. The image stack of the dorsal rib (IGPB Wijk10-246) consists of 1500 images and was recorded at a voltage of 120 kV and a current of 90 mA, yielding a voxel size of 36.69 µm. The image stack of the "rib" osteoderm (IGPB Wijk09-551), consisting of 672 images and taken with voltage of 120 kV and current of 90 mA, and a voxel size of 45.04 µm. Data were then imported and processed using MIMICS Innovation Suite 25.0 (Materialise NV, Leuven, Belgium).

Morphological, microanatomical and histological description

Vertebrae of *Eusaurosphargis* aff. *dalsassoi*.—*Morphological description*: The vertebrae show elongation of the slightly anteriorly inclined tp (Fig. 1A) which is characteristic for *Eusaurosphargis* (Scheyer et al. 2017). The centra are slender and small, ventrally constricted, and deeply amphicoelous (Fig. 1A$_2$). The neural spine is very low, forming a broadened and rugose table, which is covered by an elongated oval osteoderm (Fig. 1A; Scheyer et al. 2017, 2019). The tp from the anterior and posterior trunk region are shorter than those from the mid-trunk region (Scheyer et al. 2017).

Microanatomical description: The µCT scan of the neck vertebrae (Fig. 1B; IGPB Wijk10-231) reveals a deeply amphicoelous centrum and a large neural canal. The neural arch has a compact layer of bone that surrounds a rather irregularly, cancellous inner structure (SOM: fig. 1, Supplementary Online Material available at http://app.pan.pl/SOM/app69-Klein_Scheyer_SOM.pdf).

The µCT scan of the complete mid-trunk vertebra IGPB Wijk06-110 reveals microanatomical details through the entire vertebra (Fig. 1A, SOM: fig. 2). Observations described on the basis of µCT data are supported and/or supplemented by the information from the thin sections (IGPB Wijk08-153, IGPB Wijk11-394) that provide a higher resolution (Fig. 2). Due to the deeply amphicoelous centrum, the anterior and posterior ¼ of the centrum is excavated, surrounded by a compact cortex (SOM: fig. 2). In its mid-part, after a short transitional area where a small cavity is visible, the centrum of IGPB Wijk06-110 is completely cancellous but does not retain a clear cavity. The thin sections of IGPB Wijk08-153 document a small central medullary cavity in the centrum that is surrounded by a medullary region. The medullary region is roughly twice the size of the cavity (Fig. 2A$_1$–A$_3$). This indicates a sampling location from the anterior transitional area along the centrum (i.e., transitional between a hollow to cancellous central centrum area). In IGPB Wijk11-394, the centrum is not preserved (Fig. 2B$_1$, B$_2$). The vertebrae from Winterswijk are non-notochordal but also deeply amphicoelous. This is visible already externally on the cervical and trunk vertebral centra and corroborated by the µCT and the thin section data (Fig. 1A$_2$, SOM: figs. 1, 2). In the µCT images of IGPB Wijk06-110, the anterior part of the neural arch appears rather compact except for the neural canal and dorsolaterally to it (SOM: fig. 2). Anteriorly, the anterior part of the neural spine is separated by sediment (i.e., its anteriorly extending over the neural arch) and by a relatively compact cortex above the excavated part of the centrum. The mid-section of the neural arch, posterior to the tp, shows a cancellous tissue surrounding the neural canal (SOM: fig. 2). The posterior vertebra, i.e. the centrum and neural arch, stays cancellous until the very end where the tissue is more compact again. The posterior part of the compact neural spine reaches ventrally deep into the neural canal. The thin sections of IGPB Wijk08-153 and IGPB Wijk11-394 show free cavities dorsolaterally to the neural canal, extending into the tp (Fig. 2). µCT data and thin sections (IGPB Wijk11-394) reveal that the central/middle part of the tp is largely hollow to cancellous along their entire length. Thus, the central or mid part of the tp is sandwiched by the cortex of the dorsal and ventral margin of the tp (Fig. 2B$_2$, B$_5$, SOM: fig. 2).

The neural canal is in IGPB Wijk06-110 anteriorly large and distinct (SOM: fig. 2). It becomes smaller along the midpart of the neural arch and not well to distinguish in its posterior part. In IGPB Wijk11-394 (Fig. 2B$_1$, B$_2$), the margin of the neural canal is preserved, indicating a large neural canal, which is also obvious from IGPB Wijk08-153 (Fig. 2A$_1$–A$_3$). As mentioned above, the base of the neural spine posteriorly extends ventrally into the neural canal, giving the latter a kidney-shape. In IGPB Wijk08-153, the sutures between centrum and neural arch rest on slightly protruding pedicels, which is not the case in the two other samples. The dorsal margin of the tp is horizontal in all samples. In IGPB Wijk08-153, the ventromedial margins are in a rough 45° angle in relation to the dorsal margins.

Fig. 2. Microanatomy and histology of dorsal vertebrae of the diapsid reptile *Eusaurosphargis* aff. *dalsassoi* Nosotti & Rieppel, 2003, from Winterswijk, → The Netherlands; Lower Muschelkalk, Vossenveld Formation, lower Anisian (Middle Triassic). **A**. IGPB Wijk08-153. A$_1$, A$_2$, two thin sections, composite photograph in normal light; A$_3$, composite photograph as in A$_1$ in polarized light; A$_4$, detail of loosely organized parallel fibred tissue and simple vascular canals in the centrum, note the towards the surface open canals; A$_5$, detail of the neural spine. **B**. IGPB Wijk11-394. B$_1$, B$_2$, two thin sections, composite photograph in normal (B$_1$) and in polarized (B$_2$) light, note that the section figured in B$_1$ is from a more posterior position than the second section, which depicts the mid of the transverse process (tp); B$_3$, detail of tissue in the transitional area between neural arch and tp in polarized light; B$_4$, detail of tissue of the dorsal part of the tp in polarized light; B$_5$, detail of the lateral end of the tp in polarized light.

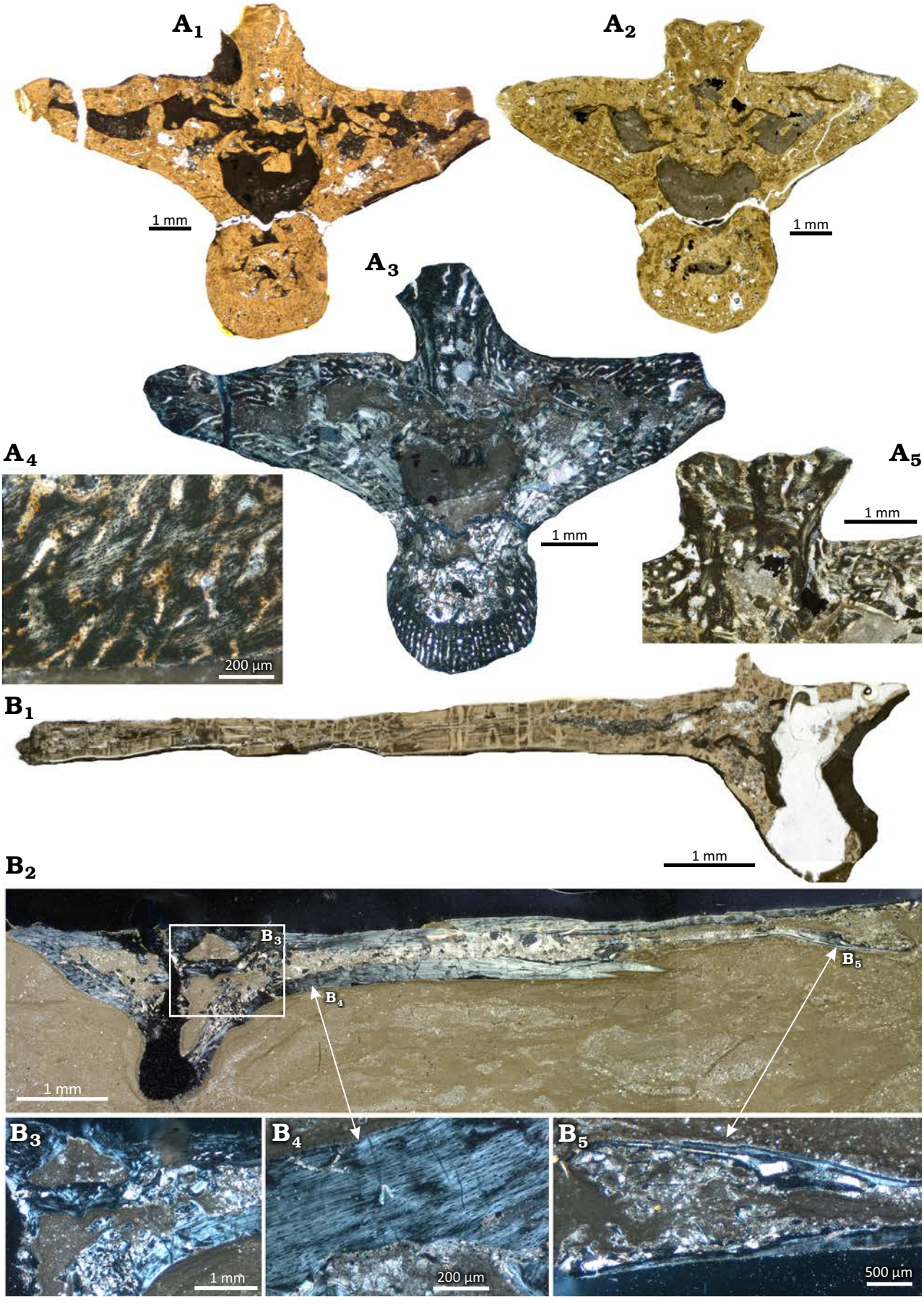
A1
1 mm
A2
1 mm
A3
1 mm
A4
200 µm
A5
1 mm
B1
1 mm
B2
B3
B4
B5
1 mm
B3
1 mm
B4
200 µm
B5
500 µm

In the two other samples, the transition of the ventromedial margins is less angled but smooth.

The neural spine of IGPB Wijk08-153 is wide at its basis and of rectangular shape (Fig. $2A_1$–A_3). In the same region, the μCT images of IGPB Wijk06-110 reveal a constricted base of the neural spine that expands dorsolaterally (SOM: fig. 2). In IGPB Wijk11-394, only the anteriormost tip of the neural spine was sampled.

Histological description: The medullary region in the centrum of IGPB Wijk08-153 consists of secondary endosteal lamellar bone forming trabeculae and/or an endosteal matrix consisting of erosion cavities surrounded by endosteal lamellar bone. Besides endosteal lamellar bone, locally few areas of calcified cartilage and accumulations of large elongated to oval shaped osteocyte lacunae are visible (Fig. $2A_3$, SOM: fig. 3A–C). Most of the margin of the medullary region is well delimited from the periosteal cortex (SOM: fig. 3A–C). However, locally erosion extends into the periosteal cortex. The dorsal part of the centrum is made of a thick layer of endosteal lamellar bone that reaches also dorsolaterally, lining here the lateral neural canal (SOM: fig. 3A–C).

The area dorsal to the neural canal, the basis of the neural spine, and dorsolaterally to the neural canal, where the tp begin, it is also formed by a similar matrix of endosteal structures but has a more cancellous appearance. Similar features are visible in the same area of Wijk11-394 (Fig. $2B_3$). The ventrolateral margin of the centrum, the ventrodorsal margins of the tp and the mid to dorsal part of the neural spine are formed by periosteal compact cortex (Fig. $2A_3$, A_4).

The periosteal tissue in Wijk08-153 is made of parallel-fibered bone with numerous but small and flat osteocyte lacunae (Fig. $2A_3$–A_5). The tissue is less organized and well vascularized by radially, reticularly, and longitudinally oriented simple vascular canals in IGPB Wijk08-153. In IGPB Wijk11-394, the tissue is distinctly higher organized, locally maybe even grading into lamellar bone, and it is largely avascular (Fig. $2B_3$–B_5). However, the section of IGPB Wijk11-394 from the more posterior region shows some long (radial) simple vascular canals, similar to those in Wijk08-153 (Fig. $2A_4$).

The lateral margins of the neural spine are each lined by a layer of parallel-fibred tissue that is more organized compared to the enclosed and much less organized parallel fibered tissue (Fig. $2A_5$). The outer layer also contains traces of fiber attachment. The dorsal part of the neural spine and the ventromedial margin of the tp of IGPB Wijk08-153 show some higher organized layers that might represent growth marks (SOM: fig. 3D).

Rib of *Eusaurosphargis* aff. *dalsassoi*.—The rib was described and figured in detail in Klein and Sichelschmidt (2014). The rib was sampled at four locations (Figs. 1E, 3). The primary cortex of the rib consists of parallel-fibred tissue (Fig. 3). The proximal section of the rib is oval with a pointed anterior tip (Fig. 3A). The section is ventrally crushed due to a morphological groove/indentation at the rib. The cross section shows a large central cavity now filled by calcite crystals. The margin of the medullary cavity is lined by a thin layer of endosteal bone. Except for the ventral part of the anterior pointed tip, where few longitudinal simple vascular canals occur, the cortex is avascular. Four alternating layers of different degrees of organization can be distinguished, representing a cyclicity. Whether the cyclicity is annual or not cannot be said based on the present data. Osteocyte lacunae are thick and very numerous in the lesser organized layers and still numerous but less thick in the more highly organized layers.

The sample proximal to the uncinate process (Fig. 3B) is elliptical. It has a split narrow medullary cavity, which is separated medially by a medullary region of endosteal bone. Below the ventral cavity the anterior periosteal cortex is made of a loosely organized parallel-fibred tissue and the region contains some large erosion cavities. Differently organized layers of tissue are only locally visible. The number of osteocyte lacunae is high in the dorsal tip. The tissue has some large longitudinal simple vascular canals that show at their margins the beginning of erosion of the cortex.

The sample through the uncinate process (Fig. $3C_1$) has a similar structure. Its medullary cavities are even more narrow which might be partially due to compaction. It shows four larger cavities along its center, which are separated by periosteal cortex. The ventral cavity is lined by a layer of endosteal bone. The middle part, mainly at the ventral side shows large simple round to oval and radial vascular canals that are lined by an erosional margin. Similar structures are also visible in the section taken from the area of the uncinate process (Fig. $3C_3$). The tissue is low organized coarse parallel-fibred tissue. Osteocyte lacunae are most numerous and fat in the anterior ventral half.

The distalmost section (Fig. 3D) has a free central medullary cavity extending from the dorsal to the ventral part. It is surrounded by a medullary region consisting of endosteal lamellar bone and erosion cavities. The cortex is highly organized but coarse parallel-fibred tissue and scattered by few longitudinal simple vascular canals. The overall number of osteocyte lacunae is clearly less when compared to the more proximal sections 1–3.

Osteoderms.—*Eusaurosphargis* is known to have different morphological types of osteoderms in different body regions (Scheyer et al. 2017). The cervical vertebrae carry long and conical spiky osteoderms (Fig. 1B, SOM: fig. 1), which, along the thoracic vertebral series, become more oblong at the base, and decrease in height until only the rugose base remains (see mid-trunk vertebra in Fig. $1A_1$; Nosotti and Rieppel 2003; Scheyer et al. 2017). Besides the row above the vertebral column, the dorsal ribs each carry an osteoderm above their respective uncinate processes (Nosotti and Rieppel 2003; Klein and Sichelschmidt 2014; Scheyer et al. 2017; Fig. 1D, E) but this feature is not unique to the genus, because similar rib-osteoderm associations are also known

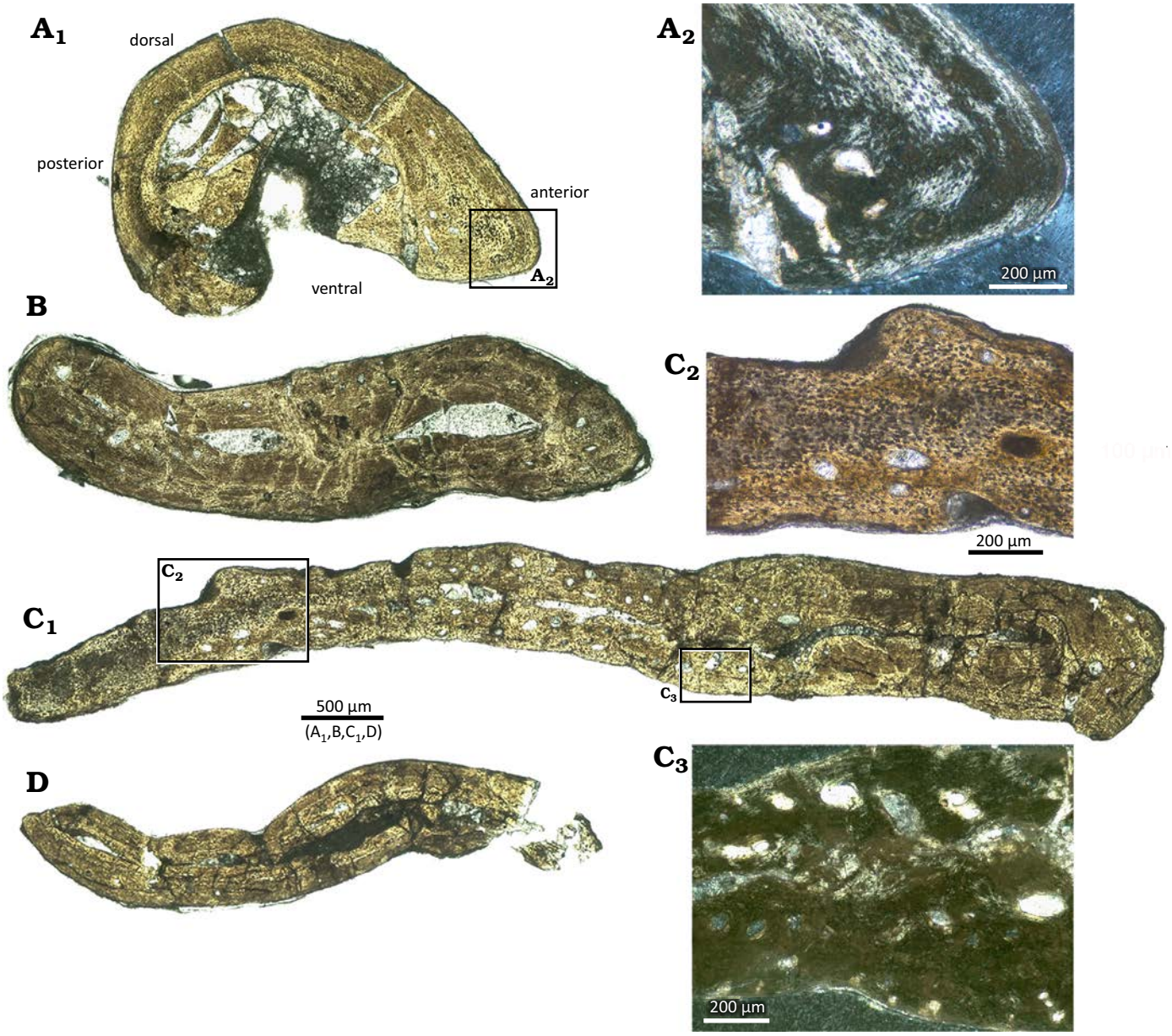

Fig. 3. Microanatomy and histology of the dorsal rib (IGPB Wijk10-246) of the diapsid reptile *Eusaurosphargis* aff. *dalsassoi* Nosotti & Rieppel, 2003, from Winterswijk, The Netherlands; Lower Muschelkalk, Vossenveld Formation, lower Anisian (Middle Triassic). Photographs of thin sections of the four different sampling locations along the rib shaft (see Fig. 1E) in normal light (A–D). **A**. Proximal part (A_1) and detail of tissue in the anterior part of the proximal rib sample in polarized light (A_2). **B**. Part anterior to the uncinate process. **C**. Part across the uncinate process (C_1), detail of tissue of the area of the uncinate process in normal light (C_2) and in polarized light (C_3). **D**. Distal end of rib shaft.

in Saurosphargidae (e.g., Li et al. 2014; Scheyer et al. 2022). The "rib" osteoderms in *Eusaurosphargis* aff. *dalsassoi* are conical with a round to oval-shaped flaring base that is set off from the dorsal part of the osteoderm (Fig. 1D). The base of the osteoderm is strongly excavated and has a festooned margin. The medial margin is convex and the lateral one concave, leading to an off-centered apex, which tapers and points slightly laterally.

The limbs of *Eusaurosphargis* are also covered by multiple osteoderms that can overlap each other in a shingle-like fashion (Scheyer et al. 2017). These "appendicular" osteoderms are superficially similar to the "rib" osteoderms except that the round-flaring base is smaller, the apex is more distinctly pointed laterally, and due to their overlapping, they are generally excavated internally (Fig. 1C).

In all three types of osteoderms, the external surfaces show some slight sculpturing (Figs. $4A_1$–A_4, 5). The osteoderms along the vertebral column are only finely pitted by small grooves, whereas the osteoderms covering the dorsal ribs and limbs show a more distinct sculpture by deeper grooves (Fig. 1B–D). At the base of the "rib" osteoderm, the external sculpture is most pronounced, often forming larger irregular tubercles. The internal bone surface of the rib osteoderm appears rough and irregular in the thin sections

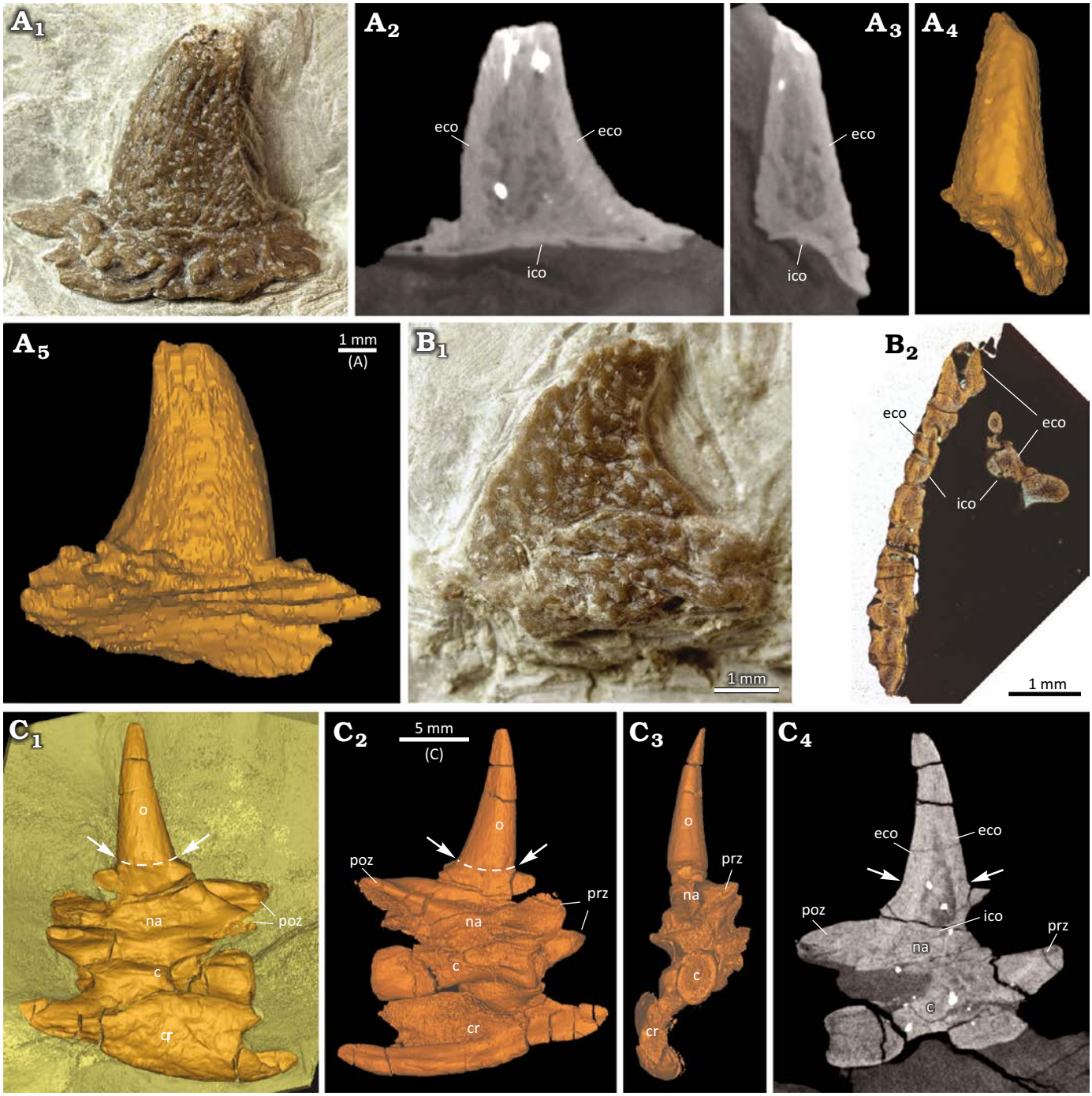

Fig. 4. Comparison of the diapsid reptile *Eusaurosphargis* aff. *dalsassoi* Nosotti & Rieppel, 2003, osteoderm external anatomy and microanatomy from Winterswijk, The Netherlands; Lower Muschelkalk, Vossenveld Formation, lower Anisian (Middle Triassic). **A**. Photograph (A_1), slice images (A_2, A_3), and surface renderings (A_4, A_5) of "rib" osteoderm IGPB Wijk09-551. A central cavity is surrounded by internal and external cortical bone. **B**. Photograph (B_1) and image of thin section (B_2) of "appendicular" osteoderm IGPB Wijk07-74. Note deep excavation of internal side of osteoderm and lack of a large central cavity. **C**. Surface renderings (C_1–C_3) and slice image (C_4) of cervical vertebra IGPB Wijk10-231 with spiky "neck" osteoderm and left cervical rib attached to the centrum. Transitional zone of neural arch and osteoderm indicated by white arrows and stippled white lines. Abbreviations: c, centrum; cr, cervical rib; eco, external cortex; ico, internal cortex; na, neural arch; o, osteoderm; poz, postzygapophysis; prz, prezygapophysis.

($5A_1$–A_5) due to vascular canals opening onto and small bony protrusions extending from the bone surface. Shallow grooves and pits are also visible in the flattened lateral osteoderms, which have not been sampled herein (Nosotti and Rieppel 2003 and Scheyer et al. 2017). From all thin sectioned osteoderms the very apex is broken off.

Microanatomical description: As described above, the "neck", "appendicular", and "rib" osteoderms differ in external morphology (Fig. 1B–D, SOM: figs. 1, 4) and do so also in their internal microstructure (Fig. 4). The base of the "appendicular" osteoderm (based on thin section) is strongly excavated and has a festooned margin. An internal

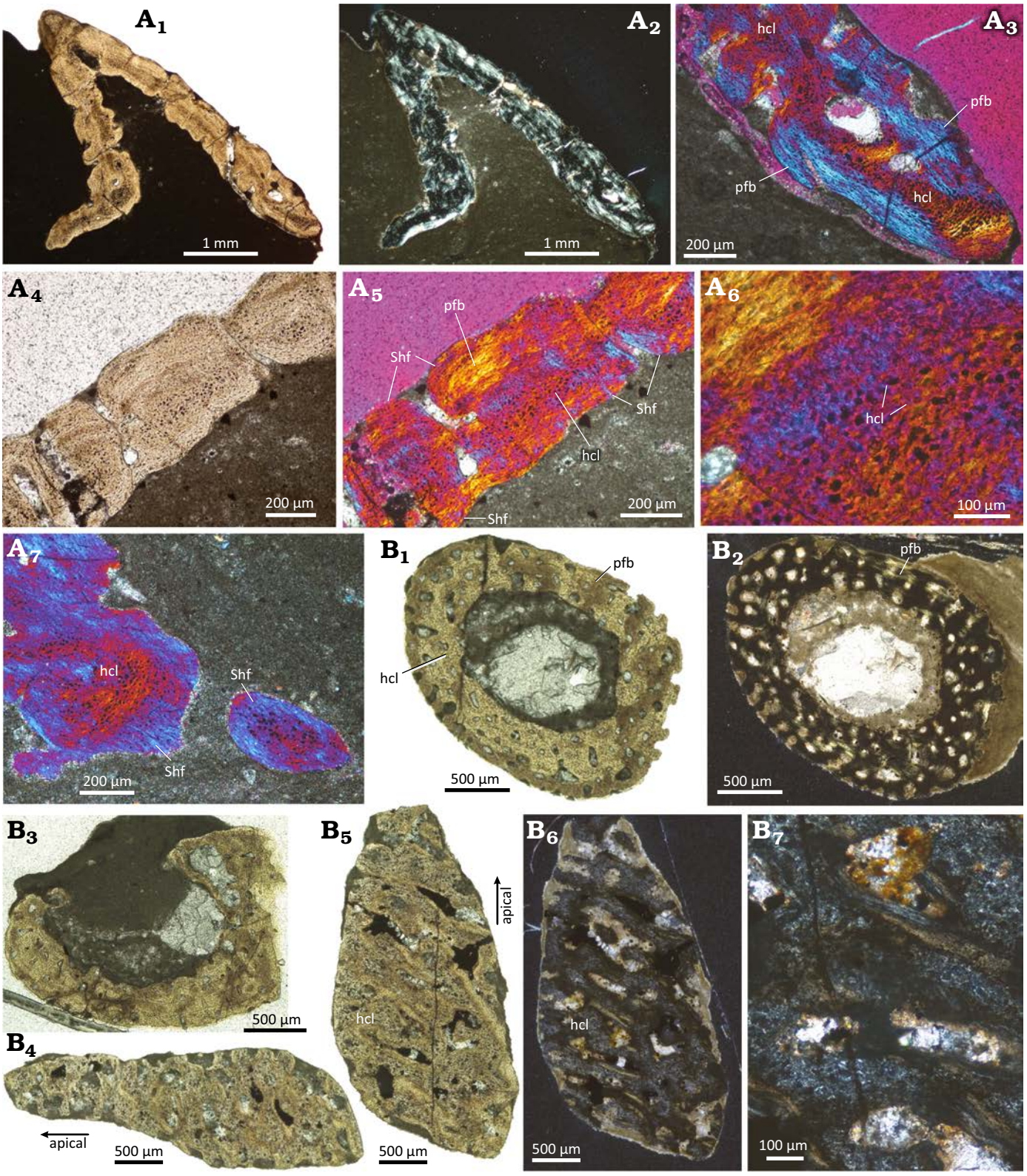

Fig. 5. Histological images of the diapsid reptile *Eusaurosphargis* aff. *dalsassoi* Nosotti & Rieppel, 2003, "appendicular" and "rib" osteoderms from Winterswijk, The Netherlands; Lower Muschelkalk, Vossenveld Formation, lower Anisian (Middle Triassic). **A**. "Appendicular" osteoderm IGPB Wijk07-74 (A_1, A_2), details (A_3–A_7). Note internal "dark" band of large and plump hypertrophied cell lacunae, surrounded by parallel-fibered bone. **B**. "Rib" osteoderm IGPB Wijk09-551 (B_1–B_3, horizontal sections through the whole osteoderm; B_4–B_7, tangential sections through apical cortex). Note central large cavity surrounded by well-vascularized cortical tissue. Abbreviations: hcl, hypertrophied cell lacunae; pfb, parallel-fibered bone; Shf, Sharpey's fibers. A_1, A_4, B_1–B_5 in normal transmitted light, A_2, B_6, and B_7 in cross-polarized light, and A_3 and A_5–A_7 in cross-polarized light with lambda filter applied.

cancellous bone or a central cavity is thus missing. The spiky "neck" and "rib" osteoderms (based on μCT data) have a central large cavity, extending from just above the base to the distal tip, but which is completely surrounded by a thick cortex, also at their base. Thus, one main difference between these and the "appendicular" osteoderm is that the latter has a deeply excavated base and lacks a large central cavity. The "rib" osteoderm has a bony base with which it attaches to the uncinate process of the rib (Figs. 1E, $5A_1$, A_2). There is no fusion or suturing between uncinate process and osteoderm, indicating only a soft-tissue connection between these bones. The "neck" osteoderm, on the other hand, lacks a broadened base and instead is rooted onto a broadened and rugose spine table of the vertebral arch. Both bones appear fused, so that a separation of osteoderm and neural arch is mostly not traceable in the scan data and only weakly visible externally (see Fig. 4C).

Histological description of the "appendicular" osteoderm: Due to the strong excavation of the base, the osteoderm flanks have an overall similar thickness (Fig. $5A_1$, A_2). The bone tissue in the flanks, the base, and the apex is mostly compact. Interior cancellous parts are absent. Only in the apical and basal regions, a few scattered larger vascular cavities are present (Fig. $5A_1$–A_3). Scattered primary simple vascular canals are found throughout the bone, usually opening on the bone surface as small foramina (Fig. $5A_4$, A_5). The external, internal, and marginal bone cortices are composed of parallel-fibered bone, rich in flattened and elongated cell lacunae (Fig. $5A_5$, A_6). Fine Sharpey's fibers are present in both internal and external cortices (Fig. $5A_5$). Within the excavated surface of the osteoderm, these fibers often insert perpendicularly or at high angles into the parallel-fibered bone, and they often accumulate in the sculpture saddles. Coarser Sharpey's fibers are most conspicuous in the base of the osteoderms (Fig. $5A_7$).

The interior part of the osteoderm appears as an irregular "band" in thin section, reflecting a sinuous three-dimensional tissue, which extends from the base to the apex (Fig. $5A_2$–A_6). In normal transmitted light, this tissue is characterized by closely spaced large to hypertrophied and plump cell lacunae in a granular, fibrous matrix (Fig. $5A_6$). The cell lacunae appear either translucent or darkly stained. In cross-polarized light, this tissue is only weakly birefringent, while adding the lambda compensator reveals a fine cross-hatching pattern of mineralized fibers with different spatial organization ("bluish and yellowish/reddish" fibers) surrounding the enlarged cell lacunae (Fig. $5A_6$).

Histological description of the "rib" osteoderm: In both cross sections (Fig. $5B_1$–B_3), the cortices are roughly about the same thickness and surround a large cavity. The cortex is formed by parallel-fibred tissue and is in both cross sections regularly and densely packed with numerous, large simple vascular canals of mainly roundish shape (Fig. $5B_1$–B_3). Some canals open up onto the internal and others onto the external cortices. The tissue contains numerous small osteocyte lacunae. Sharpey's or any fibers are not observed.

The longitudinally cut sections are from the apical region of the osteoderm and section the cortical bone tangentially (Fig. $5B_4$–B_7). As such, one section provides only a smaller cortical portion than the other section (Fig. $5B_4$, B_5). Their cortices show large simple vascular canals surrounded by parallel-fibered tissue and an interstitial matrix, a tissue with enlarged cellular structures, identified here as cell lacunae (Fig. $5B_6$, B_7, SOM: fig. 5).

Neural arches of *Saurosphargis* aff. *voltzi*.—NHMS WT647 (Fig. 6) represents two articulated neural arches, whose centra are both missing. Although slightly broken ventrally, the remains of the pedicels are broad and massive, extending parallel over the entire length of the respective neural arch. The neural arches are broad but very flat due to compaction. The neural spines were low/absent and each is covered by an osteoderm of which the oval (anteriorly and posteriorly slightly tapering) base is still firmly attached to the neural arch/spine (Fig. $6A_1$). The broken off base of the osteoderms reveals a cancellous microstructure. The typical elongated tp are constricted close to the neural arch but broaden and thicken laterally. They are overall straight and are not anteriorly inclined as in *Eusaurosphargis* aff. *dalsassoi* (Figs. 1A, 2). The preserved lateral end is a thick oval, i.e., slightly clubbed-shaped. In ventral view, the surface of the tp is smooth, and the processes are three dimensionally preserved. In ventral view, the tp are embedded in a thin bony layer that surrounds the tp dorsally except for their lateral end (Fig. 6A). In dorsal view, the separation into a surrounding thin sheath and a massive tp is not visible (Fig. $6A_1$). In dorsal view, the tp are laterally striated and distinctly compressed.

The fossil (Fig. $6A_1$) and the μCT data (Fig. $6C_2$) reveal a cancellous inner structure of the preserved part of the osteoderms. The latter are firmly attached with their bases to the neural arches (Fig. $6A_1$).

In dorsoventral view, the tp is encompassed by a thin but distinct layer of highly organized, likely lamellar bone (Fig. $6C_3$). Medial to this line the tp has a cancellous inner structure, and the lateral part is a thin bony sheath. Along its mediolateral direction the tp is encompassed by a dorsal bony layer and a much thicker ventral bony layer, leaving the inner of the tp largely cancellous or even hollow. The dorsal

Fig. 6. Two articulated neural arches of dorsal vertebrae (NHMS WT647) of *Saurosphargis* aff. *voltzi* Huene, 1936, from Themar quarry, near Schleusingen, Thuringia, Germany; Lower Muschelkalk, Jena Formation, lower Anisian (Middle Triassic). **A**. Photograph in dorsal (A_1) and ventral (A_2) views. Note the remains of the basis of the osteoderms along the midline (A_1) and the sutures to the broken off centra and the thin bony sheath (A_2). **B**. Rendered surface model images of the neural arches in dorsal (B_1), ventral (B_2), anterior (B_3), posterior (B_4), and angled dorsolateral (B_5) views. The central oval structure is plasticine with which the specimens were fixed during μCT scanning. **C**. μCT images through the neural arches; μCT picture through the middle of the anterior neural arch (C_1); μCT images through the neural arches from their dorsal to their ventral part (C_2–C_5). Abbreviations: o, osteoderm; tp, transverse process. B, C not to scale. →

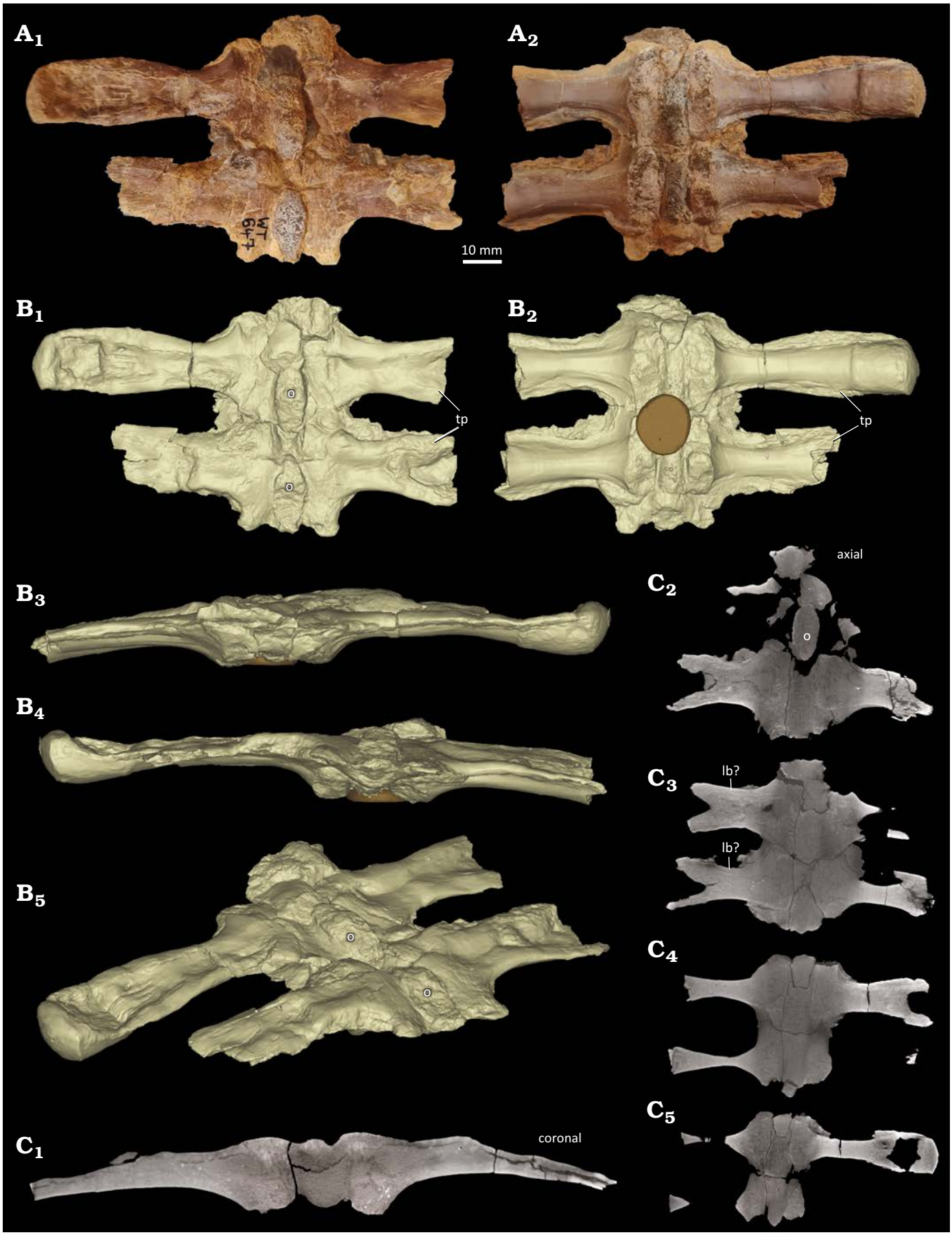
A1
A2
MT 6474
10 mm
B1
B2
o
tp
o
tp
tp
B3
B4
B5
o
o
C1
coronal
axial
C2
o
C3
lb?
lb?
C4
C5

and ventral sides are both convex. Laterally, the dorsal part of the tp is crushed/collapsed, which is well visible in the μCT pictures (Fig. 6B_1, B_4, B_5, C_5). The dorsal part is now concave and pressed into the hollow and/or cancellous center.

As far as comparable due to preparation and preserved view, the tp of mid-trunk vertebrae of *Sinosaurosphargis yunguiensis* Li et al., 2011, are quite similar to NHMS WT647. They both share the medial constriction, a bony sheath in ventral view and a club shaped lateral end (Li et al. 2011: fig. 3B). Whether these similarities are phylogenetically related or have a functional/morphological reason cannot be clarified at the moment. The tp of dorsal vertebrae of *Largocephalosaurus* (Li et al. 2014: fig. 2C) are more slender and do not show a bony sheath in ventral view. The neural arches of *Prosaurosphargis yingzishanensis* (Wolniewicz et al. 2023) are also slenderer and do not show the bony sheath in ventral view. Interestingly, the preserved two neural arches are also broken off of their centra (Wolniewicz et al. 2023: fig. 3).

Discussion

Ontogenetic stage of sampled elements.—Due to the lack of comparable samples, the histology of the sampled elements of *Eusaurosphargis* aff. *dalsassoi* does not provide reliable information on the ontogenetic stage. Tissue is in all samples, except for the osteoderms, highly organized and poorly vascularized but distinct growth marks throughout the samples are absent.

The currently known maximum width of a mid-trunk vertebra of *Eusaurosphargis* aff. *dalsassoi* from Winterswijk is around 6.5 cm (measured along the tp). These measurements are based on the mid-trunk vertebrae associated with slab NMNHL RGM 449487A (Sander et al. 2014). The ontogenetic stage of this individual is not known. The μCT scanned vertebra IGPB Wijk06-110 measures 6.3 cm, which is close to the maximal known size. The incompletely preserved mid-trunk vertebra IGPB Wijk11-394 measured ~5 cm before sampling, which is somewhat smaller than the maximal known size. Vertebra IGPB Wijk08-153 has shorter tp due to a different anatomical position but based on its centrum length, it is within a similar size range as IGPB Wijk11-394.

The dorsal rib measures 2.5 cm, which is the typical size for isolated ribs of *Eusaurosphargis* aff. *dalsassoi* from the locality of Winterswijk. Contrary to the vertebrae of *Eusaurosphargis* aff. *dalsassoi*, thoracic ribs carrying uncinate processes (which can be of various shapes, see Scheyer et al. 2017), are extremely rare in Winterswijk (Klein and Sichelschmidt 2014). Unfortunately, no rib with an uncinate process is identified associated with the vertebrae on slab NMNHL RGM 449487A.

Based on comparison with the holotype and referred specimens of *Eusaurosphargis dalsassoi* from Italy and Switzerland (e.g., Nosotti and Rieppel 2003; Scheyer et al. 2017), the studied osteoderms from Winterswijk of *Eusaurosphargis* aff. *dalsassoi* are all very small and likely derived from smaller individuals. In fact, they are in similar size range when compared to the respective elements from the juvenile specimen of the Prosanto Formation (Scheyer et al. 2017).

Both neural arches of NHMS WT647 are incomplete. The anterior one however, has the left tp completely preserved. It measures from its lateral end to the middle of the osteoderm 5.8 cm, giving an extrapolated value for the entire width of about 11.6 cm.

The size range of *S. voltzi* is difficult to assess because the holotype and only known specimen is lost. Huene (1936) figured the specimen without a scale, just stating that it was printed roughly about ½ of original size. Based on this information, NHMS WT647 is about ⅓ larger when compared to the holotype. In any case, NHMS WT647 belonged to an advanced, likely adult ontogenetic stage, although the upper size range is not known. The very compressed tp indicate poor ossification, which might be a general feature (i.e., by retaining a hollow or very spongious structure even during adult growth stages) of the taxon or might indicate a not fully grown individual.

Vertebrae and rib.—A comparison of microanatomical and osteohistological characters of *Eusaurosphargis* aff. *dalsassoi* samples from Winterswijk is hampered by the lack of comparable material such as samples of Saurosphargidae (Li et al. 2014).

The μCT data of NHMS WT647 (Fig. 6) in comparison to the μCT data of the dorsal vertebra IGPB Wijk06-110 (Fig. 2) and the thin sections revealed a similar cancellous inner structure of the neural arch and tp. However, due to a different morphology, i.e., the anteroposteriorly extending bony sheath in *Saurosphargis* aff. *voltzi*, the distribution of compact bone surrounding the tp is different when compared to *Eusaurosphargis* aff. *dalsassoi*.

A detailed comparison to contemporaneous marine reptile taxa such as sauropterygians and thalattosaurs is difficult due to difference in morphology of the respective sampled elements.

The comparison of vertebral and rib osteohistology is restricted to small Eosauropterygia (pachypleurosaurs, nothosaurs; Klein et al. 2019) and few samples of thalattosaurs (Klein et al. 2023) due to the lack of comparable histological studies of similar sized and contemporaneous taxa.

The tissue (parallel-fibred bone) and vascular pattern (longitudinal, reticular and radial orientation; simple vascular canals; partially primary osteons in eosauropterygians) is similar in small Eosauropterygia (pachypleurosaurs, nothosaurs; Klein et al. 2019) and some thalattosaurs (Klein et al. 2023) but the parallel-fibred tissue is more highly organized in *Eusaurosphargis* aff. *dalsassoi*. Further, the distribution of the periosteal and endosteal tissue is different. In thalattosaurs, no large cavities are visible (Klein et al. 2023), whereas the central cavity and the neural canal are much larger and better delimited in Eosauropterygia (Klein et al

2019). Contrary to marine reptiles, large amounts of calcified cartilage, as well as any Sharpey's fibers are absent in the vertebrae and rib of *Eusaurosphargis* aff. *dalsassoi*.

The centra of *Eusaurosphargis* aff. *dalsassoi* from Winterswijk are non-notochordal but deeply amphicoelous. Many marine reptiles such as ichthyosaurs, thalattosaurs, and some sauropterygians have amphicoelous vertebrae in which the centra show an anterior and a posterior concavity. Following Klein et al. (2019), retaining a notochordal canal in the center of the centrum (through which the notochord would extend) could further be interpreted as an adaptation to an aquatic lifestyle (i.e., as paedomorphosis). A personal inspection by one of us (TMS) of the holotype (Nosotti and Rieppel 2003) and the Ducan specimen (Scheyer et al. 2017) revealed a similar "non-notochordal but deeply amphicoelous" condition in their vertebrae. This is however not well visible due to preservation and articulation, respectively. On the basis of histology and microanatomy studied here, we found no further clear signal contradicting or supporting a secondary aquatic adaptation in *Eusaurosphargis* aff. *dalsassoi.*

Osteoderms.—*Morphological comparison*: The sampled *Eusaurosphargis* aff. *dalsassoi* osteoderms differ in shape, microanatomy, and histology from other osteoderms of diapsid reptiles. Whereas osteoderms with tapering apices (and often excavated bases) are also found in early branching thyreophoran and ankylosaurid dinosaurs (e.g., Main et al. 2005; Hayashi et al. 2010; Burns and Currie 2014), their microanatomy and histological features are very much distinct in showing separated compact cortices and cancellous cores, the former often with extensive meshwork of structural fibre bundles (see Scheyer and Sander 2004). A close association with vertebral spines or uncinate processes on the ribs is not present in this group of dinosaurs. Shingle-like osteoderms that partially overlap adjacent ones are found also in a range of squamates, such as in cordylid, anguid, and scincid lizards (e.g., Williams et al. 2022), but these are usually not deeply excavated. On the other hand, *Eusaurosphargis* osteoderms lack unornamented anterior bars (in the overlapping zone), as well as any hypermineralised tissues (such as osteodermine; see Buffrénil et al. 2011) or composite organization.

Pseudosuchian osteoderms can resemble *Eusaurosphargis* aff. *dalsassoi* osteoderms in shape and their osteoderms are often overlapping, as evidenced by the paravertebral osteoderms of crocodylians and the paramedian (and dorsal accessory) osteoderms seen for example in aetosaurs and rauisuchians. The microanatomy and histology of these osteoderms can be quite diverse (for a summary, see Scheyer 2024), often being influenced by strong external bone surface sculpturing (e.g., pitting patterns, ridges and valleys, keels, etc.). The strongly irregular surface sculpturing of the *Eusaurosphargis* aff. *dalsassoi* osteoderms, both internally and externally, are, to our knowledge, not documented for squamate or pseudosuchian osteoderms.

Among Mesozoic marine reptiles, Saurosphargidae and Placodontia are the two groups which also exhibit extensive body armour. Saurosphargidae (i.e., the Chinese genus *Largocephalosaurus* and the European *Saurosphargis*) also carry larger osteoderms associated with the neural spines and rib uncinate processes, and at least *Largocephalosaurus* and *Sinosaurosphargis* sp. also have smaller ossicles covering large parts of the body, as in a knight's chainmail (e.g., Cheng et al. 2012; Li et al. 2011, 2014). The latter are missing in *Eusaurosphargis dalsassoi* (Scheyer et al. 2017). Unfortunately, comparative histological data on the larger saurosphargid osteoderms—although different in shape from *Eusaurosphargis*, are so far unavailable (but see scan data on *Saurosphargis* aff. *voltzi* neural arches herein). Among Placodontia, Cyamodontoidea carry extensive turtle-like armour, often organized in a dorsal main carapace and in some species also a pelvic shield and ventral plastron, consisting of sutured individual bony plates (e.g., Rieppel 2002; Scheyer 2010). Suturing of osteoderms is not seen in *Eusaurosphargis*. Apart from cyamodontoids, fossils of the genus *Placodus* carry a single row of non-sutured ossifications dorsal to their neural spines (Drevermann 1933; Jiang et al. 2008), but these are more globular in shape and lack a clear base, compared with the pylon-shaped vertebral osteoderms of *Eusaurosphargis* (Nosotti and Rieppel 2003; Scheyer et al. 2017).

Hypotheses related to the nature of the interior osteoderm tissue.—The osteoderms of *Eusaurosphargis* aff. *dalsassoiare* in a histological view quite unique as described above. Four hypotheses concerning the nature of the interior tissue structure of the *Eusaurosphargis* aff. *dalsassoi* osteoderms are discussed here: (i) The interior part of the osteoderm consists of woven bone tissue (wfb); (ii) The interior parts consist of interwoven structural fiber tissue (isf); (iii) The interior part consists of postcranial fibro-cartilaginous bone (pfcb); (iv) The interior part consists of chondroid bone (cb).

Hypothesis 1 (wfb): Being one of the major tissue types found in the vertebrate skeleton, wfb, results from generally fast static bone accretion, as is usually found in fetal and early juvenile bones or as the initial bone deposition after a bone fracture (e.g., Buffrénil and Quilhac 2021; Houssaye et al. 2021). The tissue is characterized by randomly arranged collagenous fibers and scattered and randomly arranged, plump and round-shaped osteocyte lacunae (Francillon-Vieillot et al. 1990). In thin-sections, the random arrangement of the tissue is identifiable by its monorefringence or general isotropy under cross-polarized light in all three dimensions (e.g., Francillon-Vieillot et al. 1990; Stein and Prondvai 2014).

In the *Eusaurosphargis* aff. *dalsassoi* osteoderm samples, although the interior tissue studied appears mostly dark in polarized light because of spatial disorganization of the crystallite structure, it is still weakly birefringent. Surrounding the cell lacunae, a bright cross-hatching pattern is visible when applying the lambda compensator (i.e., distinct coloration of the surrounding matrix), which is usually

not observable in wfb (e.g., Woodward et al. 2014; Buffrénil and Quilhac 2021: fig. 8.8), nor are the osteocyte lacunae scattered and randomly arranged in our samples. The differences in birefringence of the more internal vs. more external tissues, the former including the large to hypertrophied cell lacunae surrounded by a fine fibrous cross-hatching pattern, are thus interpreted to be fundamental histological features.

Hypothesis 2 (isf): The isf usually consists of fiber bundles which are organized in some form of cross-hatching pattern (e.g., Scheyer and Sander 2004). The isf tissue generally shows birefringence which is stronger than that observed here. Similarly, the spatial orientation of the associated fibers and fiber bundles of the isf are usually more organized. In contrast, isf has so far not been found associated with hypertrophied cell lacunae, and its matrix is usually not granular.

Hypothesis 3 (pfcb): The pfcb consists of bone spiculae or needles embedded in a fibrous calcified cartilage matrix (Scheyer 2007). In pfcb, hypertrophied cell lacunae are present, surrounded by a fine cross-hatched pattern of fibers that appear alternately bluish and yellowish/reddish when seen in polarized light and lambda compensator. The hypertrophied cells are arranged in sub-parallel rows, similar to the cartilaginous cells of the growth plates in mammalian long bones (Scheyer 2007). Furthermore, the tissue matrix has a granular texture.

Hypothesis 4 (cb): The cb shows histological characteristics intermediate between bone and cartilage, with cartilage-like cell lacunae in a bony matrix. The tissue is widespread in earlier developmental stages in various amniotes (see Beresford 1981, 1993; and Hall 2005 for an overview of earlier studies discussing the presence of chondroid and chondroid bone in the vertebrate skeleton), but its formation and developmental origins remain largely obscure (e.g., Bailleul et al. 2016; Prondvai et al. 2020; Buffrénil and Quilhac 2021).

In the *Eusaurosphargis* aff. *dalsassoi* osteoderm samples, the differences in birefringence of the more internal vs. more external tissues, the former including large to hypertrophied cell lacunae surrounded by a fine fibrous cross-hatching pattern, are fundamental histological features. The size of the cell lacunae measurable in the thin-sections fall in the range of lacuna sizes for example of hypertrophied chondrocytes in modern articular cartilage (e.g., Zhang et al. 2012). A possible reason for microanatomical differences in the sampled *Eusaurosphargis* aff. *dalsassoi* specimens, including for example the absence of bone spiculae in the "appendicular" osteoderm, can be explained by the minute dimensions of the element and its geometry lacking a central cavity. To our assessment, the combination of these features (i.e., non-isotropy of the tissue; presence of enlarged cell lacunae) clearly rule out hypotheses 1 and 2. The presence of similar structures in pfcb and cb and the interior osteoderm tissue presented herein support hypothesis 3 and 4, in which case the hypertrophied cell lacunae could be interpreted to have housed chondrocytes (trapped cartilage cells) instead of osteocytes in the living animal.

The pfcb was so far described only in a limited sample of placodont armor plates (Scheyer 2007), so the histological characteristics of the group largely remain enigmatic (see Scheyer and Klein 2021). Scheyer (2007) hypothesized that a potential participation of trunk neural crest cells could have led to the incorporation of pfcb during placodont armour plate formation. The organized nature of the pfcb with mostly parallel-trending vascular canals in an extensive fibrocartilaginous matrix is not observed in the *Eusaurosphargis* aff. *dalsassoi* samples.

The cb, on the other hand, commonly occurs in dermal bones of the cranium and mandibles of various tetrapods (e.g., Beresford 1981, 1993; Hall 2005), usually in pre- or early postnatal ontogenetic stages, and it gets later replaced by bone tissue (e.g., Vickaryous and Hall 2008; Bailleul et al. 2016; Buffrénil and Quilhac 2021 and references therein). Furthermore, chondroid bone is involved in the early formation of the baculum of various mammalian species (e.g., Beresford 1981; Herdina et al. 2010), a less mineralized penile bone derived from postcranial connective tissue (e.g., Stockley 2012). Even in the formation of postcranial osteoderms of *Alligator mississippiensis*, the presence of chondroid bone was postulated (Dubansky and Dubansky 2018). Chondroid bone could also look very similar to cementum, another intermediate tissue (between bone and dentine) occurring in the vertebrate skeleton (e.g., Hall 2005). The latter is associated with cranial remains, usually as an anchoring tissue between teeth and alveolar bone, that can be acellular (lacking cementocytes) to cellular. As we are dealing here exclusively with postcranial remains, a potential confusion is ruled out.

Together with the assumed early developmental stage of the sampled *Eusaurosphargis* aff. *dalsassoi* osteoderms, this lends further support to hypothesis 4, in which the peculiar osteoderm histology observed herein would be largely based on the presence of chondroid bone.

Conclusions

The observed microanatomical and osteohistological differences of *Eusaurosphargis* aff. *dalsassoi* gave no clear signal towards or contrary to a secondary aquatic adaptation. The life style of *Eusaurosphargis* aff. *dalsassoi* cannot be unequivocally addressed by our sample and a semiaquatic life style cannot be ruled out. The lack of a chordal canal in *Eusaurosphargis* aff. *dalsassoi* in the current study supports a terrestrial or semiaquatic life style rather than a purely aquatic one for *Eusaurosphargis* aff. *dalsassoi*; as was already hypothesized for *Eusaurosphargis dalsassoi* based on morphological observations by Scheyer et al. (2017) and Renesto et al. (2020). Furthermore, chondroid bone (evidenced by hypertrophied chondrocyte-like cell lacunae in a bony matrix) is identified in the osteoderms of

Eusaurosphargis aff. *dalsassoi*, potentially underscoring the early ontogenetic nature of said osteoderms. Although chondroid bone tissues are widespread among vertebrates from fish to mammals, and thus its developmental and evolutionary origins could be postulated to reach back well into the Palaeozoic, we here report the oldest evidence of chondroid bone tissue in osteoderms of an extinct tetrapod from the Triassic. We thus expand the knowledge of such intermediate tissues further into deep time of vertebrate evolution by actual fossil evidence.

Acknowledgements

We would like to thank Sibelco Europe MineralsPlus Winterswijk, which operates the Winterswijkse Steengroeve, and its manager Gerard ten Dolle for access to the quarry and the support provided on their premises. We also thank all members of the Muschelkalk Workgroup for their various support over the years as well as the numerous students who helped during the excavations. We are grateful to Ralf Werneburg (NHMS) who gave permission to loan and micro-Ct-scan the *Saurosphargis* aff. *voltzi* material under his care. Olaf Dülfer (IGPB) and Christoph Wimmer-Pfeil (Staatliches Museum für Naturkunde Stuttgart, Germany) are acknowledged for the preparation of the thin sections. Georg Oleschinski (IGPB) took the photographs of the specimens. Finally, we would like to thank Alida Bailleul (Institute of Vertebrate Paleontology and Paleoanthropology, Beijing, China) and one anonymous reviewer, as well as the editors for their various efforts and help to improve the previous versions of the article.

References

Bailleul, A.M., Nyssen-Behets, C., Lenglé, B., Hall B.K., and Horner, J. R. 2016. Chondroid bone in dinosaur embryos and nestlings (Ornithischia: Hadrosauridae): Insights into the growth of the skull and the evolution of skeletal tissues. *Comptes Rendus Palevol* 15: 49–64.

Beresford, W.A. 1981. *Chondroid Bone, Secondary Cartilage and Metaplasia*. 454 pp. Urban and Schwarzenberg, Baltimore.

Beresford, W.A. 1993. Cranial skeletal tissues: diversity and evolutionary trends. *In*: B.K. Hall (ed.), *The Skull, Vol. 2. Patterns of Structural and Systematic Diversity,* 69–130. University of Chicago Press, Chicago.

Buffrénil, V. de and Quilhac, A. 2021. Bone tissue types: a brief account of currently used categories. *In*: V. de Buffrénil, A. de Ricqlès, L. Zylberberg, K. Padian, M. Laurin, and A. Quilhac (eds.), *Vertebrate Skeletal Histology and Paleohistology*, 147–182. CRC Press, Boca Raton.

Buffrénil, V. de, Dauphin, Y., Rage, J.-C., and Sire, J.-Y. 2011. An enamel-like tissue, osteodermine, on the osteoderms of a fossil anguid (Glyptosaurinae) lizard. *Comptes Rendus Palevol* 10: 427–437.

Buffrénil, V. de, Ricqlès, A. de, Zylberberg, L., Padian, K., Laurin, M., and Quilhac, A. 2021. *Vertebrate Skeletal Histology and Paleohistology*. 825 pp. CRC Press, Boca Raton.

Burns, M.E. and Currie, P.J. 2014. External and internal structure of ankylosaur (Dinosauria, Ornithischia) osteoderms and their systematic relevance. *Journal of Vertebrate Paleontology* 34: 835–851.

Cheng, L., Chen, X., Zeng, X., and Cai, Y. 2012. A new eosauropterygian (Diapsida: Sauropterygia) from the Middle Triassic of Luoping, Yunnan Province. *Journal of Earth Science* 23: 33–40.

Drevermann, F. 1933. Die Placodontier. 3. Das Skelett von *Placodus gigas* Agassiz im Senckenberg-Museum. *Abhandlungen der Senckenbergischen Naturforschenden Gesellschaft* 38: 321–364.

Dubansky, B.H. and Dubansky, B.D. 2018. Natural development of dermal ectopic bone in the American alligator (*Alligator mississippiensis*) resembles heterotopic ossification disorders in humans. *The Anatomical Record* 301: 56–76.

Dülfer, O. and Klein, N. 2006. Studentische Lehrgrabung im Winterswijker Muschelkalk. *Der Präparator* 52: 90–96.

Francillon-Vieillot, H., Buffrénil, V. de, Castanet, J., Géraudie, J., Meunier, F.J., Sire, J.Y., Zylberberg, L., and Ricqlès, A. de. 1990. Microstructure and mineralization of vertebrate skeletal tissues. *Skeletal Biomineralization: Patterns, Processes and Evolutionary Trends* 1: 471–530.

Hagdorn, H. and Simon, T. 2010. Vossenveld-Formation. *In*: *Lithostratigraphisches Lexikon der Deutschen Stratigraphischen Kommission. BGR, Hannover* [available from: https://litholex.bgr.de/pages/Einheit.aspx-?ID=45].

Hall, B.K. 2005. *Bones and Cartilage. Developmental and Evolutionary Skeletal Biology*. 760 pp. Elsevier Academic Press, Amsterdam.

Hayashi, S., Carpenter, K., Scheyer, T.M., Watabe, M., and Suzuki, D. 2010. Function and evolution of ankylosaur dermal armor. *Acta Palaeontologica Polonica* 55: 213–228.

Heijne, J., Klein, N., and Sander, P.M. 2019. The uniquely diverse taphonomy of the marine reptile skeletons (Sauropterygia) from the Lower Muschelkalk (Anisian) of Winterswijk, The Netherlands. *Paläontologische Zeitschrift* 93: 1–24.

Herdina, A.N., Herzig-Staschil, B., Hilgers, H., Metscher, B.D., and Plenk, H., Jr. 2010. Histomorphology of the penis bone (baculum) in the gray long-eared bat *Plecotus austriacus* (Chiroptera, Vespertilionidae). *The Anatomical Record* 293: 1248–1258

Houssaye, A., Davesne, D., and Canoville, A. 2021. A methodological renaissance to advance perennial issues in vertebrate paleohistology. *In*: V. d. Buffrénil, A. d. Ricqlès, L. Zylberberg, K. Padian, M. Laurin, and A. Quilhac (eds.), *Vertebrate Skeletal Histology and Paleohistology*, 793–798. CRC Press, Boca Raton.

Huene, F., von. 1936. *Henodus chelyops*, ein neuer Placodontier. *Palaeontographica Abteilung A* 84: 99–148.

Jiang, D.-Y., Motani, R., Hao, W.-C., Rieppel, O. Sun, Y.-L, Schmitz, L., and Sun, Z.-Y. 2008. First record of Placodontoidea (Reptilia, Sauropterygia, Placodontia) from the Eastern Tethys. *Journal of Vertebrate Paleontology* 28: 904–908.

Klein, N. and Sander, P.M. 2007. Bone histology and growth of the prosauropod dinosaur *Plateosaurus engelhardti* von Meyer, 1837 from the Norian bonebeds of Trossingen (Germany) and Frick (Switzerland). *Special Papers in Palaeontology* 77: 169–206.

Klein, N. and Sichelschmidt, O.J. 2014. Remarkable dorsal ribs with distinct uncinate processes from the early Anisian of the Germanic Basin (Winterswijk, The Netherlands). *Neues Jahrbuch für Geologie und Paläontologie Abhandlungen* 271: 307–314.

Klein, N., Canoville, A., and Houssaye, A. 2019. Microstructure of vertebrae, ribs, and gastralia of Triassic sauropterygians: New insights into the microanatomical processes involved in aquatic adaptations of marine reptiles. *The Anatomical Record* 302: 1770–1791.

Klein, N., Sander, P.M., Liu, J., Druckenmiller, P., Metz, E.T., Kelley, N. P., and Scheyer, M.T. 2023. Comparative bone histology of two thalattosaurians (Diapsida: Thalattosauria): *Askeptosaurus italicus* from the Alpine Triassic (Middle Triassic) and a Thalattosauroidea indet. from the Carnian of Oregon (Late Triassic). *Swiss Journal of Paleontology* 142: 15.

Li, C., Jiang, D.-Y., Cheng L., Wu, X.-C., and. Rieppel, O. 2014. A new species of *Largocephalosaurus* (Diapsida: Saurosphargidae), with implications for the morphological diversity and phylogeny of the group. *Geological Magazine* 151: 100–120.

Li, C., Rieppel, O., Wu, X.-C., Zhao, L.-J., and Wang, L.-T. 2011. A new Triassic marine reptile from southwestern China. *Journal of Vertebrate Paleontology* 31: 303–312.

Main, R.P., Ricqlès, A. de., Horner, J.R., and Padian, K. 2005. The evolution and function of thyreophoran dinosaur scutes: implications for plate function in stegosaurs. *Paleobiology* 31: 291–314.

Nosotti, S. and Rieppel, O. 2003. *Eusaurosphargis dalsassoi* n. gen n. sp., a new, unusual diapsid reptile from the Middle Triassic of Besano (Lombardy, Italy). *Memoire della Società Italiana di Scienze Naturali e del Museo Civico di Storia Naturale di Milano* 31: 3–33.

Prondvai, E., Witten, P.E., Abourachid, A., Huysseune, A., and Adriaens, D. 2020. Extensive chondroid bone in juvenile duck limbs hints at accelerated growth mechanism in avian skeletogenesis. *Journal of Anatomy* 236: 463–473.

Renesto, S., Kustatscher, E., and Gianolla, P. 2020. A putative juvenile specimen of *Eusaurosphargis dalsassoi* from the Anisian (Middle Triassic) of Piz da Peres (Dolomites, Northern Italy). *Rivista Italiana di Paleontologia e Stratigrafia* 126: 249–259.

Rieppel, O. 1995. Fragmenta Sauropterygiana. *Neues Jahrbuch für Geologie und Paläontologie Abhandlungen* 197: 383–397.

Rieppel, O. 2002. The dermal armor of the cyamodontoid placodonts (Reptilia, Sauropterygia): Morphology and systematic value. *Fieldiana: Geology, New Series* 46: 1–41.

Oosterink, H.W., Klein, N., Diependaal, H., and Sander, P.M. 2021. Der Untere Muschelkalk von Winterswijk. *In*: N. Hauschke, M. Franz, and G.H. Bachmann (eds.), *Trias – Aufbruch in das Erdmittelalter, Vol. 2*, 416–421. Verlag Dr. Friedrich Pfeil, Munich.

Sander, P.M., Klein, N., Albers, P.C.H., Bickelmann, C., and Winkelhorst, H. 2014. Postcranial morphology of a basal Pistosauroidea (Sauropterygia) from the Lower Muschelkalk of Winterswijk, The Netherlands. *Paläontologische Zeitschrift* 88: 55–71.

Scheyer, T.M. 2007. Skeletal histology of the dermal armor of Placodontia: the occurrence of "postcranial fibro-cartilaginous bone" and its developmental implications. *Journal of Anatomy* 211: 737–753.

Scheyer, T.M. 2010. New interpretation of the postcranial skeleton and overall body shape of the placodont *Cyamodus hildegardis* Peyer, 1931 (Reptilia, Sauropterygia). *Palaeontologia Electronica* 13 (2): 15A.

Scheyer, T.M. 2024. The pseudosuchian record in paleohistology: a small review. *The Anatomical Record* [available online, https://doi.org/10.1002/ar.25455].

Scheyer, T.M. and Klein, N. 2021. Sauropterygia: Placodontia. *In*: V. de Buffrénil, A. de Ricqlès, L. Zylberberg, K. Padian, M. Laurin, and A. Quilhac (eds.), *Vertebrate Skeletal Histology and Paleohistology*, 425–434. CRC Press, Boca Raton.

Scheyer, T.M. and Sander, P.M. 2004. Histology of ankylosaur osteoderms: implications for systematics and function. *Journal of Vertebrate Paleontology* 24: 874–893.

Scheyer, T.M., Klein, N., Sichelschmidt, O., Neenan, J.M., and Albers, P. 2019. With plates and spikes—the heavily armoured *Eusaurosphargis* aff. *dalsassoi*. *Grondboor & Hamer* (*Staringia* 16) 73: 216–221.

Scheyer, T.M., Neenan, J.M., Bodogan, T., Furrer, H., Obrist, C., and Plamondon, M. 2017. A new, exceptionally preserved juvenile specimen of *Eusaurosphargis dalsassoi* (Diapsida) and implications for Mesozoic marine diapsid phylogeny. *Scientific Reports* 7: 4406.

Scheyer, T.M., Oberli, U., Klein, N., and Furrer, H. 2022. A large osteoderm-bearing rib from the Upper Triassic Kössen Formation (Norian/Rhaetian) of eastern Switzerland. *Swiss Journal of Palaeontology* 141: 1.

Stein, K. and Prondvai, E. 2014. Rethinking the nature of fibrolamellar bone: an integrative biological revision of sauropod plexiform bone formation. *Biological Reviews* 89: 24–47.

Stockley, P. 2012. The baculum. *Current Biology* 22: R1032–R1033.

Vickaryous, M.K. and Hall, B.K. 2008. Development of the dermal skeleton in *Alligator mississippiensis* (Archosauria, Crocodylia) with comments on the homology of osteoderms. *Journal of Morphology* 269: 398–422.

Voeten, D.F.A.E., During, M.A.D., Lankamp, J., and Smit, J. 2019. The Middle Triassic Vossenveld formation in Winterswijk—an uniquely preserved Anisian ecosystem along the western shore of the Muschelkalk sea. *Grondboor & Hamer* (*Staringia* 16) 73: 1–300.

Wachtler, M. 2018. A new reptile from the Middle Triassic (Anisian) of Piz da Peres (Dolomites—Northern Italy). *In*: T. Perner and M. Wachtler (eds.), *Some New and Exciting Triassic Archosauria from the Dolomites (Northern Italy)*, 9–16. Dolomythos-Museum, Innichen.

Willemse, D.M., Willemse, N.W., and Voeten, D.F.A.E. 2019. An aff. *Eusaurosphargis* vertebra associated with an isolated dentary. *Grondboor & Hamer* (*Staringia* 16) 73: 273–277.

Williams, C., Kirby A., Marghoub, A., Kéver, L., Ostashevskaya-Gohstand, S., Bertazzo S., Moazen, M., Abzhanov, A., Herrel, A., Evans, S.E., and Vickaryous, M. 2022. A review of the osteoderms of lizards (Reptilia: Squamata). *Biological Reviews* 97: 1–19.

Wolniewicz, A., Shen, Y., Li, Q., Sun, Y., Qiao, Y., Chen, Y., Hu, Y.-W., and Liu, J. 2023. An armoured marine reptile from the Early Triassic of South China and its phylogenetic and evolutionary implications. *eLife* 12: e83163

Woodward, H.N., Horner, J.R., and Farlow, J.O. 2014. Quantification of intraskeletal histovariability in *Alligator mississippiensis* and implications for vertebrate osteohistology. *PeerJ* 2: e422.

Zhang, W., Chen, J., Zhang, S., and Ouyang, H.-W. 2012. Inhibitory function of parathyroid hormone-related protein on chondrocyte hypertrophy: The implication for articular cartilage repair. *Arthritis Research & Therapy* 14: 221.